Dirac point phonons at high-symmetry points: Towards materials realization

Yu Feng,[1,2] Chengwu Xie,[2] Hong Chen ⦿,[2] Ying Liu,[3,*] and Xiaotian Wang[2,4,†]

[1]*School of Physics and Electronic Engineering, Jiangsu Normal University, Xuzhou 221116, China*
[2]*School of Physical Science and Technology, Southwest University, Chongqing 400715, China*
[3]*School of Materials Science and Engineering, Hebei University of Technology, Tianjin 300130, China*
[4]*Institute for Superconducting and Electronic Materials (ISEM), University of Wollongong, Wollongong 2500, Australia*

Dirac point semimetals and related Fermi arc surface states are extremely important in topological electronic systems. In 2021, Chen *et al.* [Phy. Rev. Lett. **126**, 185301 (2021)] proposed that Dirac points can appear on high-symmetry lines (HSLs) or at high-symmetry points (HSPs) in three-dimensional (3D) phonon systems as an extension from Dirac points in electronic systems. Inspired by this work, we present an exhaustive list of Dirac point phonons (DPPs) at HSPs in 230 space groups (SGs) by checking the encyclopedia of emergent particles in 3D crystals. The DPPs are divided into four categories: charge-zero (C-0) DPPs, charge-two (C-2) DPPs, quadratic DPPs (QDPPs), and cubic crossing DPPs (CCDPPs). 29 SGs, 6 SGs, 19 SGs, and 5 SGs are identified as candidate SGs for obtaining C-0 DPPs, C-2 DPPs, QDPPs, and CCDPPs at HSPs, respectively. Importantly, herein we contribute to the realization of materials with DPPs at HSPs and through the following: (i) we propose five realistic materials, namely, $Pna2_1$-type Li_3AsS_3, $P2_1$-type NiSbS, $P\bar{4}2_1c$-type NaBH$_4$, and $Pm\bar{3}n$-type Ti$_3$Au and Ta$_3$Sn as materials with C-0 DPPs, C-2 DPPs, QDPPs, and CCDPPs at HSPs, respectively, based on the first-principles calculations. The surface states for these five materials are also examined in this work. (ii) We present 626 candidates with C-0 DPPs, 183 candidates with C-2 DPPs, 433 candidates with QDPPs, and 102 candidates with CCDPPs at HSPs, which were discovered by checking the phonon dispersions of 10 037 materials listed in the phonon database at Kyoto University. (iii) Due to the materials with SGs 103, 104, 106, 158, 184, 222, 223, 226, and 228 are not included in the phonon database at Kyoto University, we propose 18 candidates with C-0 DPPs, 5 candidates with QDPPs, and 8 candidates with CCDPPs at HSPs with above-mentioned SGs by screening the Inorganic Crystal Structure Database (ICSD). Therefore, our findings can be used to guide research into Dirac points at HSPs in 3D phonon systems.

I. INTRODUCTION

Topological materials have been extensively studied theoretically and experimentally in the last decade because of their fundamental and practical importance [1–5]. Topological semimetals [6–13] with band degeneracies have received significant attention among other topological materials since Weyl semimetals [14–17] were proposed and predicted to carry interesting surface states and novel quantum responses. In addition to Weyl semimetals, other types of topological semimetals have been reported based on symmetry analysis and first-principles calculations, including Dirac semimetals [18–26], threefold, sixfold, and eightfold degenerate nodal point semimetals [27–37], nodal line semimetals [38–46], and nodal surface semimetals [47–50]. The Fermi-Dirac distribution has also been noted to govern electrons. In topological semimetals, topological signatures (i.e., band degeneracies) must be close to the Fermi level to be detectable or manifest in physical properties because the involved energy scale is usually much less than the Fermi energy. However, phonons are spinless bosons that follow the Bose–Einstein statistics. For phonons, there is no concept of Fermi level. This could be advantageous for topological phonons (TPs) because the entire spectrum is experimentally accessible, and the phonon band degeneracies anywhere in the spectrum can be analyzed in principle. Furthermore, in phonon systems, the spinless Bloch functions are invariant under an even number of $\mathcal{T}$ operations, i.e., $\mathcal{T}^2 = 1$. Hence, phonons are an excellent platform for investigating spinless topological behaviors. A few realistic materials have recently been proposed as topological phononic materials [51–75], and some of them have been confirmed experimentally [69,75]. For example, there have been reports on Weyl point phonons (WPPs) [51–58], Weyl complex phonons [59,60], triple point phonons [61], sixfold degenerate nodal point phonons [62], Dirac phonons [63], nodal line phonons [64–72], and nodal surface phonons [73,74]. The double Weyl points in FeSi [75] and the nodal lines in MoB$_2$ [69] have also been detected experimentally using inelastic x-ray scattering, which provided a strong driving force for the field.

Remarkably, in 2021, Chen *et al.* [63] identified 27 space groups (SGs) as candidate SGs for searching for

———
*Corresponding author: ying_liu@hebut.edu.cn
†Corresponding author: xiaotianwang@swu.edu.cn

TABLE I. The first column contains the SGs with DPPs at HSPs mentioned in Ref. [63]. The second column contains the SGs of the realized materials in Ref. [63]. The third column contains the added SGs with DPPs at HSPs that were included in Ref. [11]. The DPPs are divided into four categories: C-0 DPPs, C-2 DPPs, QDPPs, and CCDPPs.

SGs with DPPs at HSPs mentioned by Chen *et al.* in Ref. [63]	SGs of the realized materials in Ref. [63]	Added SGs with DPPs at HSPs in Ref. [11]	
52, 54, 56, 60, 73, 124, 126, 128, 130, 133, 135, 137, 138, 142, 163, 165, 167, 176, 192, 193, 194, 206, 222, 223, 226, 228, and 230	52, 60, 73, 124, 137, 138, 142, 194, and 230	C-0 DPPs	29, 33, 103, 104, 110, 158, 159, 161, 184, 185, 219, and 220
		C-2 DPPs	19, 92, 96, 198, 212, and 213
		QDPPs	106, 114, 184, 185, 186, 188, and 190
		CCDPPs	218 and 220

three-dimensional (3D) Dirac point phonons (DPPs) at high-symmetry points (HSPs) by screening their symmetry conditions. Based on high-throughput calculations, they [63] also proposed some Dirac point phononic materials with 9 out of the 27 SGs (see Table I). We would like to point out that Yu *et al.* [11] have already accomplished a complete list of emergent particles in 3D crystals. Usually, the DPPs at HSPs can be classified into four categories: charge-zero (C-0) DPPs, charge-two (C-2) DPPs, quadratic DPPs (QDPPs), and cubic crossing DPPs (CCDPPs). Figure 1 presents the schematics of these four types of DPPs. By checking the encyclopedia of emergent particles in 3D crystals, we identified 29 SGs, 6 SGs, 19 SGs, and 5 SGs as candidate SGs for searching for C-0 DPPs, C-2 DPPs, QDPPs, and CCDPPs at HSPs, respectively. As shown in Table I, some SGs are not mentioned in Ref. [63].

Note that DPPs should be much more common in 3D materials. Hence, we must propose as many material candidates with DPPs as possible to aid follow-up experimental studies [76,77]. For this purpose, in this work we contribute to the field of materials realization for the DPPs at HSPs. We first propose five realistic materials, namely, $Pna2_1$-type Li_3AsS_3, $P2_1$-type NiSbS, $P\bar{4}2_1c$-type $NaBH_4$, and $Pm\bar{3}n$-type Ti_3Au and Ta_3Sn, as hosts with C-0 DPPs, C-2 DPPs, QDPPs, and CCDPPs, respectively, in their phonon dispersions. Moreover, we show the arc-shaped phononic surface states for the above-mentioned materials. Second, we examined the phonon dispersions of 10 037 materials listed in the phonon database at Kyoto University [78] and determined 626 candidates with C-0 DPPs, 183 candidates with C-2 DPPs, 433 candidates with QDPPs, and 102 candidates with CCDPPs at HSPs. Third, there are no materials with SGs 103, 104, 106, 158, 184, 222, 223, 226, and 228 in the phonon database at Kyoto University, and thus, we screened the Inorganic Crystal Structure Database (ICSD) [79] and listed a series of material candidates with above-mentioned SGs hosting DPPs at HSPs.

Our results can aid in the efficient prediction of DPPs at HSPs using first-principles calculations and in material realization for future experimental detection.

II. COMPUTATIONAL METHODS

To determine the ground states of the five realistic materials, $Pna2_1$-type Li_3AsS_3, $P2_1$-type NiSbS, $Pm\bar{3}n$-type Ti_3Au and Ta_3Sn, and $P\bar{4}2_1c$-type $NaBH_4$, first-principles calculations were performed based on the density functional theory [80], as implemented in the Vienna *ab initio* simulation package (VASP) [81]. The exchange-correlation functional was modeled within the generalized gradient approximation (GGA) using the Perdew-Burke-Ernzerhof realization [82]. The projector augmented-wave method [83] was used to define the interactions between ions and valence electrons. The energy cutoff was set to 500 eV. A Γ-centered k mesh of $9 \times 9 \times 9$ was used for the Brillouin zone (BZ) sampling of these four materials. The energy convergence criterion was set at 10^{-6} eV. The crystal structure was totally relaxed until the maximum force on each atom was less than -0.01 eV. We used the PHONOPY package [84] to calculate the phonon dispersions of the $1 \times 1 \times 1$ Li_3AsS_3 cell and the $2 \times 2 \times 2$ NiSbS, $2 \times 2 \times 2$ Ti_3Au and Ta_3Sn, and $2 \times 2 \times 2$ $NaBH_4$ supercells based on the density functional perturbation theory (DFPT). The phonon surface states were calculated by constructing a Wannier tight-binding Hamiltonian of phonons [85]. We also shown the quality of the Wannier functions for the five realistic materials in Fig. S1 (see the Supplemental Material (SM) [86]).

III. C-0 DPPS AT HSPS

As shown in Fig. 1(a), C-0 DPPs are zero-dimensional fourfold phonon band degeneracies with a topological charge of 0. DPPs have linear dispersions along all directions in the momentum space. Note that DPPs can appear on
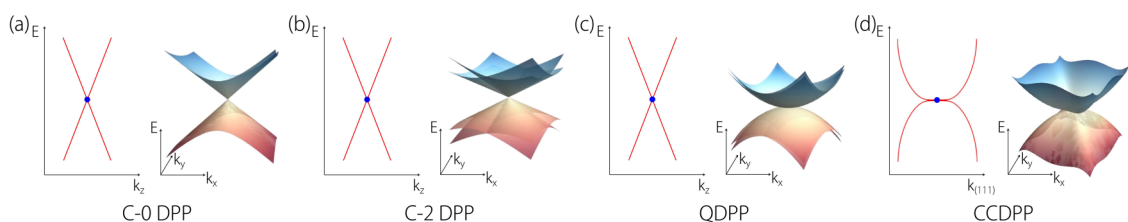
FIG. 1. Schematics of the (a) C-0 DPP, (b) C-2 DPP, (c) QDPP, and (d) CCDPP.

TABLE II. A list of the C-0 DPPs at HSPs in the 230 SGs. The first and second columns contain the SG number and SG symbol, respectively. The third column shows the name of k. The fourth and the fifth columns contain the IRRs of the LG and the GEs of the LG of k, respectively. For more details, one can refer to Refs. [11,90].

29	$Pca2_1$	T, R	$\{R_5, R_5\}$	$\{C_{2z}|\frac{1}{2}0\frac{1}{2}\}, \{\sigma_y|00\frac{1}{2}\}, \mathcal{T}$
33	$Pna2_1$	T	$\{R_5, R_5\}$	$\{C_{2z}|\frac{1}{2}\frac{1}{2}\frac{1}{2}\}, \{\sigma_y|0\frac{1}{2}\frac{1}{2}\}, \mathcal{T}$
52	$Pnna$	U	$\{R_9, R_{10}\}$	$\{\sigma_z|\frac{1}{2}\frac{1}{2}\frac{1}{2}\}, \{C_{2y}|000\}, \{I|\frac{1}{2}\frac{1}{2}0\}, \mathcal{T}$
54	$Pcca$	U	$\{R_9, R_{10}\}$	$\{\sigma_z|0\frac{1}{2}\frac{1}{2}\}, \{C_{2y}|000\}, \{I|0\frac{1}{2}0\}, \mathcal{T}$
56	$Pccn$	$U,$	$\{R_9, R_{10}\}$	$\{\sigma_x|00\frac{1}{2}\}, \{C_{2z}|000\}, \{I|\frac{1}{2}\frac{1}{2}\frac{1}{2}\}, \mathcal{T};$
		T		$\{\sigma_y|00\frac{1}{2}\}, \{C_{2z}|000\}, \{I|\frac{1}{2}\frac{1}{2}\frac{1}{2}\}, \mathcal{T}$
60	$Pbcn$	T	$\{R_9, R_{10}\}$	$\{\sigma_y|0\frac{1}{2}\frac{1}{2}\}, \{C_{2z}|000\}, \{I|\frac{1}{2}0\frac{1}{2}\}, \mathcal{T}$
73	$Ibca$	W	$\{R_9, R_9\}$	$\{E|000\}, \{C_{2z}|\frac{1}{2}0\frac{1}{2}\}, \{C_{2y}|\frac{1}{2}\frac{1}{2}0\}, \{I|000\}, \mathcal{T}$
103	$P4cc$	Z, A	$\{R_{10}, R_{10}\}$	$\{C_{4z}^+|000\}, \{\sigma_{db}|00\frac{1}{2}\}, \mathcal{T}$
104	$P4nc$	Z	$\{R_{10}, R_{10}\}$	$\{C_{4z}^+|000\}, \{\sigma_{db}|\frac{1}{2}\frac{1}{2}\frac{1}{2}\}, \mathcal{T}$
110	$I4_1cd$	P	$\{R_{10}, R_{10}\}$	$\{\sigma_{da}|\frac{1}{4}\frac{3}{4}\frac{1}{2}\}, \{C_{2z}|000\}, \{C_{4z}^+|\frac{3}{4}\frac{1}{4}\frac{1}{2}\}\mathcal{T}$
130	$P4/ncc$	R	$\{R_9, R_{10}\}$	$\{\sigma_y|00\frac{1}{2}\}, \{C_{2x}|\frac{1}{2}\frac{1}{2}0\}, \{I|\frac{1}{2}\frac{1}{2}\frac{1}{2}\}, \mathcal{T}$
138	$P4_2/ncm$	R	$\{R_9, R_{10}\}$	$\{\sigma_y|00\frac{1}{2}\}, \{C_{2x}|\frac{1}{2}\frac{1}{2}0\}, \{I|\frac{1}{2}\frac{1}{2}\frac{1}{2}\}, \mathcal{T}$
142	$I4_1/acd$	P	$\{R_{13}, R_{14}\}$	$\{S_{4z}^-|\frac{1}{2}00\}, \{E|000\}, \{C_{2y}|0\frac{1}{2}\frac{1}{2}\}, \{I|000\}\mathcal{T}$
158	$P3c1$	A	$\{R_6, R_6\}$	$\{C_3^+|000\}, \{\sigma_{v1}|00\frac{1}{2}\}, \mathcal{T}$
159	$P31c$	A	$\{R_6, R_6\}$	$\{C_3^+|000\}, \{\sigma_{d1}|00\frac{1}{2}\}, \mathcal{T}$
161	$R3c$	Z	$\{R_6, R_6\}$	$\{C_3^+|000\}, \{\sigma_{d1}|\frac{1}{2}\frac{1}{2}\frac{1}{2}\}, \mathcal{T}$
163	$P\bar{3}1c$	A	$\{R_7, R_8\}$	$\{\sigma_{d1}|00\frac{1}{2}\}, \{C_3^+|000\}, \{I|000\}, \mathcal{T}$
165	$P\bar{3}c1$	$A,$	$\{R_7, R_8\}$	$\{\sigma_{v1}|00\frac{1}{2}\}, \{C_3^+|000\}, \{I|000\}, \mathcal{T}$
		H	$\{R_6, R_6\}$	$\{C_3^+|000\}, \{C_{21}''|00\frac{1}{2}\}, \{I|000\}\mathcal{T}$
167	$R\bar{3}c$	Z	$\{R_7, R_8\}$	$\{\sigma_{d1}|\frac{1}{2}\frac{1}{2}\frac{1}{2}\}, \{C_3^+|000\}, \{I|000\}, \mathcal{T}$
184	$P6cc$	H	$\{R_6, R_6\}$	$\{C_3^+|000\}, \{\sigma_{d1}|00\frac{1}{2}\}, \{C_6^+|000\}\mathcal{T}$
185	$P6_3cm$	H	$\{R_3, R_3\}$	$\{C_3^+|000\}, \{\sigma_{d1}|000\}, \{C_6^+|00\frac{1}{2}\}\mathcal{T}$
192	$P6/mcc$	H	$\{R_7, R_8\}$	$\{\sigma_{d1}|00\frac{1}{2}\}, \{C_3^+|000\}, \{\sigma_h|000\}, \{I|000\}\mathcal{T}$
193	$P6_3/mcm$	H	$\{R_5, R_6\}$	$\{S_3^+|00\frac{1}{2}\}, \{C_{21}''|00\frac{1}{2}\}, \{I|000\}\mathcal{T}$
206	$Ia\bar{3}$	R	$\{R_7, R_7\}, \{R_8, R_9\}$	$\{C_{31}^+|000\}, \{C_{2x}|\frac{1}{2}\frac{1}{2}0\}, \{C_{2z}|\frac{1}{2}0\frac{1}{2}\}, \{I|000\}\mathcal{T}$
219	$F\bar{4}3c$	L	$\{R_6, R_6\}$	$\{C_{31}^-|000\}, \{\sigma_{db}|\frac{1}{2}\frac{1}{2}\frac{1}{2}\}, \mathcal{T}$
220	$I\bar{4}3d$	P	R_{16}	$\{C_{32}^+|0\frac{1}{2}\frac{1}{2}\}, \{C_{2y}|0\frac{1}{2}\frac{1}{2}\}, \{C_{2x}|\frac{1}{2}\frac{1}{2}0\}, \{S_{4x}^+|\frac{1}{2}00\}$
226	$Fm\bar{3}c$	L	$\{R_7, R_8\}$	$\{\sigma_{db}|\frac{1}{2}\frac{1}{2}\frac{1}{2}\}, \{C_{31}^-|000\}, \{I|\frac{1}{2}\frac{1}{2}\frac{1}{2}\}, \mathcal{T}$
228	$Fd\bar{3}c$	$L,$	$\{R_7, R_8\}$	$\{\sigma_{db}|\frac{1}{2}\frac{1}{2}\frac{1}{2}\}, \{C_{31}^-|000\}, \{I|\frac{3}{4}\frac{3}{4}\frac{3}{4}\}, \mathcal{T};$
		W	$\{R_{13}, R_{14}\}$	$\{S_{4x}^+|\frac{1}{2}\frac{1}{2}\frac{1}{2}\}, \{E|000\}, \{C_{2d}|\frac{1}{4}\frac{1}{4}\frac{1}{4}\}, \{I|\frac{3}{4}\frac{3}{4}\frac{3}{4}\}\mathcal{T}$
230	$Ia\bar{3}d$	P	$\{R_9, R_{10}\}, R_{16}$	$\{C_{32}^+|0\frac{1}{2}\frac{1}{2}\}, \{C_{2y}|0\frac{1}{2}\frac{1}{2}\}, \{C_{2x}|\frac{1}{2}\frac{1}{2}0\}, \{S_{4x}^+|\frac{1}{2}00\}, \{I|000\}\mathcal{T}$

high-symmetry lines (HSLs) or at HSPs in the 3D BZ. In this section we only focused on the DPPs at HSPs.

After analyzing the symmetry conditions and screening the encyclopedia of emergent particles [11], we discovered that the candidate SGs with the numbers 29, 33, 52, 54, 56, 60, 73, 103, 104, 110, 130, 138, 142, 158, 159, 161, 163, 165, 167, 184, 185, 192, 193, 206, 219, 220, 226, 228, and 230 are the platforms for obtaining C-0 DPPs at HSPs. Table II shows a complete list of the C-0 DPPs at HSPs in the 230 SGs. The SG numbers, SG symbols, irreducible representations (IRRs) of the little group (LG) of k, and the generating elements (GEs) of the little group (LG) of k are shown in this table. k is a high-symmetry k point or k line defined in Table 3.6 of [90].

As shown in Table I, Chen *et al.* in Ref. [63] did not mention the SGs with the numbers 29, 33, 103, 104, 110, 158, 159, 161, 184, 185, 219, and 220, which have C-0 DPPs.

Hence, in this section we use the SGs with the numbers 104 and 33 as examples to provide detailed symmetry conditions for the occurrence of C-0 DPPs at HSPs in both SGs.

The first example is the $P4nc$ (SG No. 104), in which C-0 DPPs can appear at the Z HSP. The complete point group at Z point belongs to $C_{4v}\bigotimes\{E, \mathcal{T}\}$ with E representing the identity operation and $\mathcal{T}$ representing the time-reversal symmetry. The point group C_{4v} is generated by C_{4z} and σ_{db}. In addition, as shown in Table II, there is a two-dimensional (2D) irrep R_{10}. When $\mathcal{T}$ is considered, this point is invariant under $\mathcal{T}\sigma_{db}$, where $(\mathcal{T}\sigma_{db})^2 = e^{-ik_z} = -1$ at this point. Thus, the degeneracy at this point is doubled, resulting in fourfold irreps $\{R_{10}, R_{10}\}$. On this basis, the symmetry operation (R) could adopt the following matrix representations $\mathcal{D}(R)$:

$$\mathcal{D}(C_{4z}) = i\Gamma_{03}, \quad \mathcal{D}(\sigma_{db}) = i\Gamma_{02}, \quad \mathcal{D}(\mathcal{T}) = \Gamma_{22}\mathcal{K}. \quad (1)$$

Here $\Gamma_{ij} = \sigma_i \otimes \sigma_j$, where σ is the Pauli matrix and $\mathcal{K}$ is the complex conjugation operation. Next, we characterize this fourfold degenerate point by constructing an effective Hamiltonian $\mathcal{H}_{104}$ from the symmetry constraints,

$$\mathcal{D}(R)\mathcal{H}(\boldsymbol{k})\mathcal{D}^{-1}(R) = \mathcal{H}(R\boldsymbol{k}). \tag{2}$$

Thus, the effective Hamiltonian adopts the following form:

$$\begin{aligned} \mathcal{H}_{104}(\boldsymbol{k}) = \omega(\boldsymbol{k})\Gamma_{00} + \sum_{i=1}^{3}[c_{i1}\Gamma_{i0}k_z \\ + c_{i2}\Gamma_{i1}(k_x^2 - k_y^2) + c_{i3}\Gamma_{i2}k_x k_y], \end{aligned} \tag{3}$$

indicating a fourfold degeneracy. It is worth noting that $\omega(\boldsymbol{k}) = c_0 + c_1(k_x^2 + k_y^2) + c_3 k_z^2$ is the overall energy shift, which does not influence the topology at this point. The effective model shows that it has a linear dispersion in all directions.

The second example is the $Pna2_1$ (SG No. 33), in which the C-0 DPPs can appear at the T HSP. The T point in No. 33 SG can be discussed in a similar manner as the previous example. The T point is an invariant under the combined operation $\mathcal{T}\sigma_y$. Furthermore, one could have $(\mathcal{T}\sigma_y)^2 = e^{(-ik_y)} = -1$, indicating a Kramer-like degeneracy at this point. In addition, as shown in Table II, there is a 2D irrep (R_5). Thus, the combined operation $\mathcal{T}\sigma_y$ enforces a fourfold degeneracy.

The $\boldsymbol{k} \cdot \boldsymbol{p}$ Hamiltonian of T point can be obtained by group representation theory [90]. The Herring little group of T point is G_8^5, and it generating elements are $P = \{C_{2z}|\frac{1}{2}\frac{1}{2}\frac{1}{2}\}$, $Q = \{\sigma_y|0\frac{1}{2}\frac{1}{2}\}$. The R_5 irreducible representation of G_8^5 can be written as

$$\Delta(P) = -i\sigma_2, \quad \Delta(Q) = -i\sigma_1. \tag{4}$$

Notice T point has $\mathcal{T}$, and the reality of R_5 induced space group irreducible representation belongs to case (b) in Ref. [90]. Then the matrix representation for $\{C_{2z}|\frac{1}{2}\frac{1}{2}\frac{1}{2}\}$, $\{\sigma_y|0\frac{1}{2}\frac{1}{2}\}$ and $\mathcal{T}$ can be written as

$$\mathcal{D}\left(\left\{C_{2z}|\frac{1}{2}\frac{1}{2}\frac{1}{2}\right\}\right) = \begin{pmatrix} \Delta(P) & 0 \\ 0 & \Delta(P) \end{pmatrix},$$

$$\mathcal{D}\left(\left\{\sigma_y|0\frac{1}{2}\frac{1}{2}\right\}\right) = \begin{pmatrix} \Delta(Q) & 0 \\ 0 & \Delta(Q) \end{pmatrix}, \tag{5}$$

$$\mathcal{D}(\mathcal{T}) = \begin{pmatrix} 0 & -\Delta(E)N \\ \Delta(E)N & 0 \end{pmatrix},$$

where E is the identity element and $N = i\sigma_2\mathcal{K}$ can be determined by $NN^* = -\Delta(E)$ and $\Delta(R) = N\Delta^*(\mathcal{T}^{-1}R\mathcal{T})N^{-1}$, resulting in the following effective model:

$$\begin{aligned} \mathcal{H}_{33}(\boldsymbol{k}) = c_0\Gamma_{00} + c_1\Gamma_{01}k_x \\ + c_2\Gamma_{02}k_y + \sum_{i=1}^{3}c_{i1}\Gamma_{i0}k_z, \end{aligned} \tag{6}$$

which indicates that it has a linear dispersion in all directions.

Li_3AsS_3 [91], which has a $Pna2_1$-type structure, can be obtained by reacting stoichiometric amounts of lithium, arsenic, and sulfur in a ratio of 3:1:3 in excess LiI. Figure 2(a) shows the crystal structure of Li_3AsS_3. Li_3AsS_3 crystallizes in the orthorhombic $Pna2_1$ (SG No. 33) with lattice constants of $a = 8.090$ Å, $b = 6.658$ Å, and $c = 9.868$ Å (experimental data at $20\,^\circ$C). The optimized lattice constants are $a = 8.142$ Å, $b = 6.696$ Å, and $c = 9.912$ Å, which agree well with the
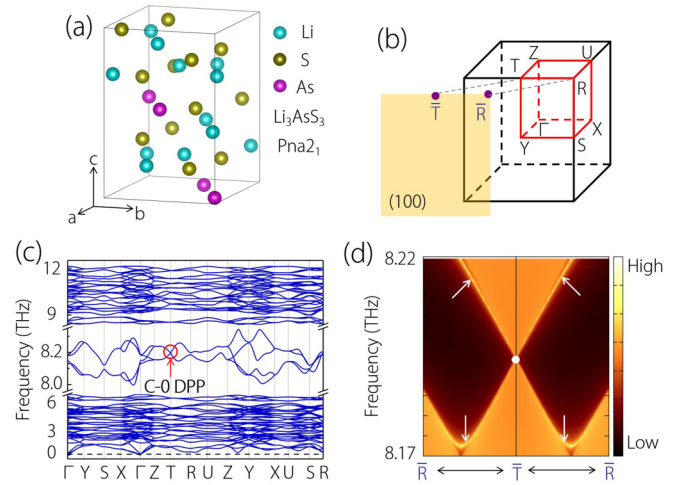
FIG. 2. (a) Crystal structure of $Pna2_1$-type Li_3AsS_3, (b) 3D BZ and 2D (100) surface BZ, (c) phonon dispersion of Li_3AsS_3 along the Γ-Y-S-X-Γ-Z-T-R-U-Z-Y-X-U-S-R paths, and (d) phonon local density of states (LDOSs) projected on the (100) surface. The white arrows indicate the phonon surface states.

experimental data [91]. The phonon dispersion of Li_3AsS_3 was obtained along the Γ-Y-S-X-Γ-Z-T-R-U-Z-Y-X-U-S-R paths [see Fig. 2(b)]. In good agreement with the above-mentioned symmetry analysis, a C-0 DPP (red circle) with a fourfold degeneracy and linear dispersion can be observed at the T HSP in the 3D BZ. Figure 2(d) shows the phonon LDOS of Li_3AsS_3 along the $\bar{R}$-$\bar{T}$-$\bar{R}$ surface path projected on the [100] surface. The white dot and white arrows indicate the positions of the projected $\bar{T}$ point and the arc-shaped phonon surface states, respectively. We would like to point out that the arc-shaped phonon surface states are not topologically protected because the C-0 DPPs have a topological charge of 0 [34].

It is worth noting that the realization of materials with C-0 DPPs is worth investigating. In Table S1 we present 644 material candidates with SG numbers 29, 33, 52, 54, 56, 60, 73, 103, 104, 110, 130, 138, 142, 158, 159, 161, 163, 165, 167, 184, 185, 192, 193, 206, 219, 220, 226, 228, and 230, which we discovered by checking the phonon database at Kyoto University [78] and ICSD [79] as hosts with C-0 DPPs at HSPs in the 3D BZ. Thus far, inelastic x-ray scattering has been used to image the topological band degeneracy in TP experiments. For example, the double Weyl points in FeSi and the nodal lines in MoB_2 were confirmed in experiments using inelastic x-ray scattering [69,75].

IV. C-2 DPPS AT HSPS

As shown in Fig. 1(b), C-2 DPPs are zero-dimensional fourfold phonon band degeneracies with a topological charge of ± 2. C-2 DPPs [55] have linear dispersions along all directions in the momentum space. C-2 DPPs can appear on HSLs or at HSPs in the 3D BZ. In this section we focus on the case of C-2 DPPs at HSPs. C-2 DPPs contain two C-1 WPPs with the same topological charge. After analyzing the symmetry conditions and screening the encyclopedia of emergent particles [11], we discovered that the candidate SGs with the numbers

TABLE III. A list of the C-2 DPPs at HSPs in the 230 SGs. The first and second columns contain the SG number and SG symbol, respectively. The third column shows the name of $\boldsymbol{k}$. The fourth and the fifth columns contain the IRRs of the LG and the GEs of the LG of $\boldsymbol{k}$, respectively. For more details, one can refer to Refs. [11,90].

19	$P2_12_12_1$	R	$\{R_5, R_5\}$	$\{C_{2z}\vert\frac{1}{2}0\frac{1}{2}\}, \{C_{2y}\vert\frac{1}{2}\frac{1}{2}0\}, \mathcal{T}$
92	$P4_12_12$	A	$\{R_6, R_7\}$	$\{C_{4z}^+\vert00\frac{1}{4}\}, \{C_{2a}\vert\frac{1}{2}\frac{1}{2}\frac{1}{4}\}, \mathcal{T}$
96	$P4_32_12$	A	$\{R_6, R_7\}$	$\{C_{4z}^+\vert00\frac{3}{4}\}, \{C_{2a}\vert\frac{1}{2}\frac{1}{2}\frac{3}{4}\}, \mathcal{T}$
198	$P2_13$	R	$\{R_4, R_4\}, \{R_5, R_6\}$	$\{C_{31}^-\vert000\}, \{C_{2x}\vert\frac{1}{2}\frac{1}{2}0\}, \{C_{2y}\vert0\frac{1}{2}\frac{1}{2}\}, \mathcal{T}$
212	$P4_332$	R	$\{R_4, R_4\}, R_8$	$\{C_{2x}\vert\frac{1}{2}\frac{1}{2}0\}, \{C_{2y}\vert0\frac{1}{2}\frac{1}{2}\}, \{C_{31}^-\vert000\}, \{C_{2b}\vert\frac{1}{4}\frac{1}{4}\frac{1}{4}\}, \mathcal{T}$
213	$P4_132$	R	$\{R_4, R_4\}, R_8$	$\{C_{2x}\vert\frac{1}{2}\frac{1}{2}0\}, \{C_{2y}\vert0\frac{1}{2}\frac{1}{2}\}, \{C_{31}^-\vert000\}, \{C_{2b}\vert\frac{3}{4}\frac{3}{4}\frac{3}{4}\}, \mathcal{T}$

19, 92, 96, 198, 212, and 213 are the platforms for obtaining C-2 DPPs at HSPs. Table III shows a complete list of the C-2 DPPs at HSPs in the 230 SGs.

In this section we present the symmetry analysis of two SGs with C-2 DPPs at HSPs as examples. The first example is the $P2_12_12_1$ (SG No. 19), which contains a C-2 DPP at the R HSP in the 3D BZ. As shown in Table IV, it is the double degeneracy of the 2D irrep (R_5) that induces such a Dirac point. Under these 4D irreps $\{R_5, R_5\}$, the matrix representations of the corresponding generating elements can be derived as

$$\mathcal{D}(C_{2z}) = i\Gamma_{02}, \quad \mathcal{D}(C_{2y}) = i\Gamma_{01}, \quad \mathcal{D}(\mathcal{T}) = -\Gamma_{22}\mathcal{K}, \quad (7)$$

such that the effective model takes the following form:

$$\mathcal{H}_{19}(\boldsymbol{k}) = c_0\Gamma_{00} + \sigma_0 \otimes (c_1k_x\sigma_1 + c_2k_y\sigma_2 + c_3k_z\sigma_3). \quad (8)$$

It can be easily deduced that each 2D irrep has a Weyl point with a topological charge of $C = 1$. Owing to the constraints from the corresponding symmetries, two Weyl points of the same chirality meet at point R, resulting in a C-2 Dirac point. It also has linear dispersions in all directions, similar to C-0 DPP; however, it has a nonzero topological charge.

The same symmetry discussion can also be applied to the $P2_13$ (SG No. 198), where the C-2 DPP can be found at the R HSP in the 3D BZ. The effective model around the band crossing at the R point can also be characterized by $\mathcal{H}_{19}$, indicating that a C-2 Dirac point is composed of two Weyl points with the same chirality. Based on the symmetry analysis, we propose a realistic material, NiSbS [92] with the $P2_13$ SG (No. 198), as a material with a C-2 DPP at the R HSP in the 3D BZ. Figure 3(a) shows its crystal structure.

TABLE IV. A list of the QDPPs at HSPs in the 230 SGs. The first and second columns contain the SG number and SG symbol, respectively. The third column shows the name of $\boldsymbol{k}$. The fourth and the fifth columns contain the IRRs of the LG and the GEs of the LG of $\boldsymbol{k}$, respectively. For more details, one can refer to Refs. [11,90].

106	$P4_2bc$	A	$\{R_{10}, R_{10}\}$	$\{C_{4z}^+\vert00\frac{1}{2}\}, \{\sigma_{db}\vert\frac{1}{2}\frac{1}{2}\frac{1}{2}\}, \mathcal{T}$
114	$P\bar{4}2_1c$	A	$\{R_{10}, R_{10}\}$	$\{S_{4z}^+\vert000\}, \{\sigma_{db}\vert\frac{1}{2}\frac{1}{2}\frac{1}{2}\}, \mathcal{T}$
124	$P4_132$	Z, A	$\{R_{12}, R_{13}\}$	$\{I\vert00\frac{1}{2}\}, \{\sigma_{db}\vert00\frac{1}{2}\}, \{C_{4z}^+\vert000\}, \mathcal{T}$
126	$P4/mcc$	Z	$\{R_{12}, R_{13}\}$	$\{I\vert\frac{1}{2}\frac{1}{2}\frac{1}{2}\}, \{\sigma_{db}\vert00\frac{1}{2}\}, \{C_{4z}^+\vert\frac{1}{2}\frac{1}{2}0\}, \mathcal{T}$
128	$P4/mnc$	$Z,$	$\{R_{12}, R_{13}\}$	$\{I\vert00\frac{1}{2}\}, \{\sigma_{db}\vert00\frac{1}{2}\}, \{C_{4z}^+\vert\frac{1}{2}\frac{1}{2}0\}, \mathcal{T};$
		A	$\{R_{12}, R_{13}\}$	$\{I\vert00\frac{1}{2}\}, \{\sigma_{db}\vert00\frac{1}{2}\}, \{S_{4z}^+\vert\frac{1}{2}\frac{1}{2}\frac{1}{2}\}, \mathcal{T}$
130	$P4/ncc$	$Z,$	$\{R_{12}, R_{13}\}$	$\{I\vert\frac{1}{2}\frac{1}{2}\frac{1}{2}\}, \{\sigma_{db}\vert00\frac{1}{2}\}, \{C_{4z}^+\vert000\}, \mathcal{T};$
		A	$\{R_9, R_{10}\}, \{R_{13}, R_{14}\}$	$\{C_{2x}\vert\frac{1}{2}\frac{1}{2}0\}, \{C_{4z}^+\vert000\}, \{I\vert\frac{1}{2}\frac{1}{2}\frac{1}{2}\}, \mathcal{T}$
133	$P4_2/nbc$	A	$\{R_{12}, R_{13}\}$	$\{I\vert\frac{1}{2}\frac{1}{2}0\}, \{\sigma_x\vert\frac{1}{2}\frac{1}{2}0\}, \{C_{4z}^+\vert\frac{1}{2}\frac{1}{2}\frac{1}{2}\}, \mathcal{T}$
135	$P4_2/mbc$	A	$\{R_9, R_{10}\}, \{R_{13}, R_{14}\}$	$\{C_{2x}\vert\frac{1}{2}\frac{1}{2}0\}, \{C_{4z}^+\vert\frac{1}{2}\frac{1}{2}\frac{1}{2}\}, \{I\vert000\}, \mathcal{T}$
137	$P4_2/nmc$	A	$\{R_{12}, R_{13}\}$	$\{I\vert\frac{1}{2}\frac{1}{2}0\}, \{\sigma_{db}\vert00\frac{1}{2}\}, \{S_{4z}^+\vert\frac{1}{2}\frac{1}{2}\frac{1}{2}\}, \mathcal{T}$
176	$P6_3/m$	A	$\{R_{13}, R_{15}\}$	$\{C_6^+\vert00\frac{1}{2}\}, \{I\vert00\frac{1}{2}\}, \mathcal{T}$
184	$P6cc$	A	$\{R_6, R_6\}, \{R_{12}, R_{12}\}$	$\{C_3^+\vert000\}, \{\sigma_{v1}\vert00\frac{1}{2}\}, \{C_2\vert000\}, \mathcal{T}$
185	$P6_3cm$	A	$\{R_6, R_{12}\}$	$\{C_3^+\vert000\}, \{\sigma_{d1}\vert000\}, \{C_2\vert00\frac{1}{2}\}, \mathcal{T}$
186	$P6_3mc$	A	$\{R_6, R_{12}\}$	$\{C_3^+\vert000\}, \{\sigma_{v1}\vert000\}, \{C_2\vert00\frac{1}{2}\}, \mathcal{T}$
188	$P\bar{6}c2$	A	$\{R_7, R_8\}$	$\{\sigma_{v1}\vert00\frac{1}{2}\}, \{C_3^+\vert000\}, \{\sigma_h\vert000\}, \mathcal{T}$
190	$P\bar{6}2c$	A	$\{R_7, R_8\}$	$\{\sigma_{d1}\vert00\frac{1}{2}\}, \{C_3^+\vert000\}, \{\sigma_h\vert000\}, \mathcal{T}$
192	$P6/mcc$	A	$\{R_7, R_8\}, \{R_{16}, R_{17}\}$	$\{\sigma_{d1}\vert00\frac{1}{2}\}, \{C_3^+\vert000\}, \{\sigma_h\vert000\}, \{C_2\vert000\}, \mathcal{T}$
193	$P6_3/mcm$	A	R_{15}	$\{C_6^+\vert00\frac{1}{2}\}, \{C_{21}'\vert000\}, \{I\vert000\}, \mathcal{T}$
194	$P6_3/mmc$	A	R_{15}	$\{C_6^+\vert00\frac{1}{2}\}, \{C_{21}''\vert000\}, \{I\vert000\}, \mathcal{T}$
222	$Pn\bar{3}n$	X	$\{R_{12}, R_{13}\}$	$\{I\vert\frac{1}{2}\frac{1}{2}\frac{1}{2}\}, \{\sigma_x\vert\frac{1}{2}\frac{1}{2}\frac{1}{2}\}, \{C_{4y}^-\vert000\}, \mathcal{T}$
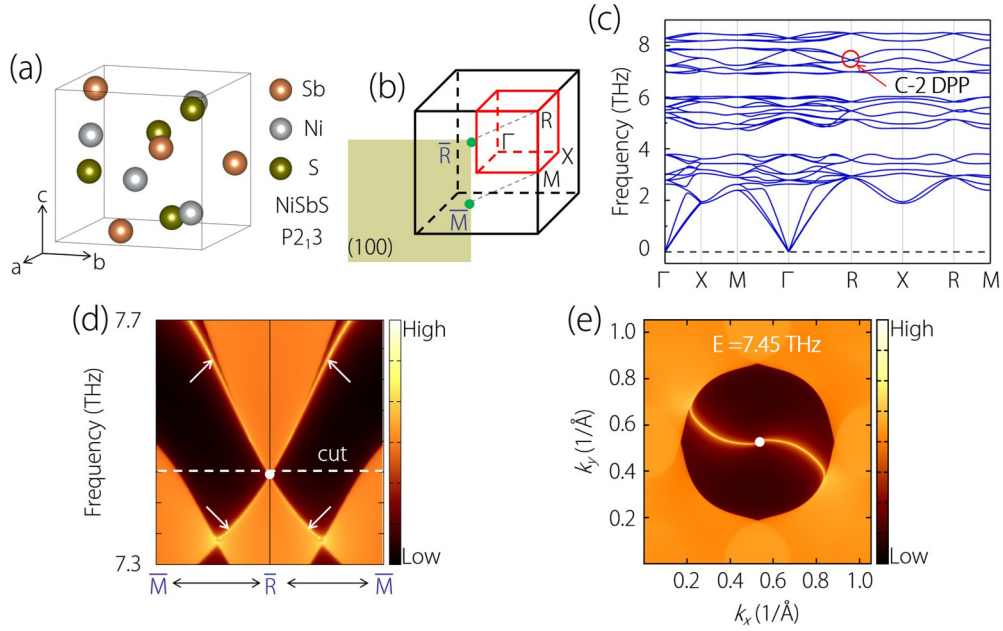
FIG. 3. (a) Crystal structure of $P2_13$-type NiSbS, (b) 3D BZ and 2D (100) surface BZ, (c) phonon dispersion of NiSbS along the Γ-X-M-Γ-R-X-R-M paths, and (d) phonon LDOS projected on the (100) surface. The white arrows indicate the phonon surface states. (e) The constant energy slice at 7.45 THz, as marked by the white dotted line in (d).

The optimized lattice constants are $a = b = c = 5.960$ Å, which match well with the experimental lattice constants of $a = b = c = 5.881$ Å [92]. Figure 3(c) depicts the phonon dispersion of NiSbS along the Γ-X-M-Γ-R-X-R-M paths [see Fig. 3(b)]. A DPP with Chern number $|C| = 2$, denoted as C-2 DPP, is highlighted with a red circle at the R HSP. The results obtained from the first-principles calculations are in good agreement with those obtained using the group theory approach (see Table III). Unlike the normal DPPs with $C = 0$ that were mentioned in Sec. III, the C-2 DPPs are topologically charged, with $|C| = 2$. A topological charge can result in many intriguing electronic, optical, and magnetic phenomena, all of which are strongly influenced by the sign of the topological charge, i.e., the chirality. Figure 3(d) shows the nontrivial phonon surface states that arise from the $\overline{R}$ point.

Furthermore, we discovered 183 material candidates with SG numbers 19, 92, 96, 198, 212, and 213 that have C-2 DPPs at HSPs in their phonon band structures by checking the phonon database at Kyoto University. Table S2 contains a list of the materials and their related SG numbers.

V. QDPPS AT HSPS

As shown in Fig. 1(c), QDPPs are zero-dimensional four-fold phonon band degeneracies with a topological charge of 0. QDPPs have linear dispersions along certain HSLs and a quadratic energy splitting in the plane normal to the HSL. QDPPs can appear on HSLs or at HSPs in the 3D BZ. In this section we focus on the QDPPs at HSPs. After analyzing the symmetry conditions and screening the encyclopedia of emergent particles [11], we discovered that the candidate SGs with the numbers 106, 114, 124, 126, 128, 130, 133, 135, 137, 176, 184, 185, 186, 188, 190, 192, 193, 194, and 222 are the platforms for obtaining QDPPs at HSPs. More details

can be found in Table IV, which contains a complete list of the QDPPs at HSPs in the 230 SGs.

We present the $P\bar{4}2_1c$ (SG No. 114), in which the QDPP only appears at the A HSP in the 3D BZ, as a typical example from the viewpoint of symmetry. As shown in Table IV, the irreps at the A point have fourfold dimensions, and a Dirac point is expected to appear at this point. On such a basis, the matrix representations of corresponding symmetry operations can be expressed as

$$\mathcal{D}(S_{4z}) = i\Gamma_{03}, \quad \mathcal{D}(\sigma_{db}) = i\Gamma_{02}, \quad \mathcal{D}(\mathcal{T}) = -\Gamma_{22}\mathcal{K}, \quad (9)$$

resulting in the effective model taking the following form:

$$\mathcal{H}_{114}(\boldsymbol{k}) = \omega(\boldsymbol{k})\Gamma_{00} + c_1\Gamma_{02}k_z$$
$$+ \sum_{i=1}^{3}[c_{i1}\Gamma_{i1}(k_x^2 - k_y^2) + c_{i2}\Gamma_{i2}k_xk_y], \quad (10)$$

which shows that it has a linear dispersion along [001] and a quadratic dispersion in the plane normal to this direction. This is known as a QDPP. Compared to the above-mentioned two types of DPPs, it has a quadratic dispersion within the k_x-k_y plane but no topological charge.

Figure 4(a) shows the crystal structure of the $P\bar{4}2_1c$-type NaBH$_4$ material [93]. The optimized lattice constants for NaBH$_4$ are $a = b = 4.334$ Å and $c = 5.892$ Å, which agree well with the experimental values ($a = b = 4.086$ Å and $c = 5.597$ Å) [93]. The H, Na, and B atoms are located at 8e (0.009, 0.768, 0.381), 2a (0.0, 0.0, 0.0), and 2a (0.0, 0.0, 0.5) Wyckoff positions, respectively. Figure 4(b) shows the 3D bulk BZ and the 2D (010) surface BZ. Figure 4(c) shows the phonon dispersion of NaBH$_4$ along the Γ-X-M-Γ-Z-R-A-Z-X-R-M-A paths. A QDPP with a fourfold degeneracy at the A HSP around 72 THz can be seen. As shown in Fig. 4(d), the QDPP has a linear dispersion along the k_z axis (i.e., M-A-M' direction) and a quadratic phonon
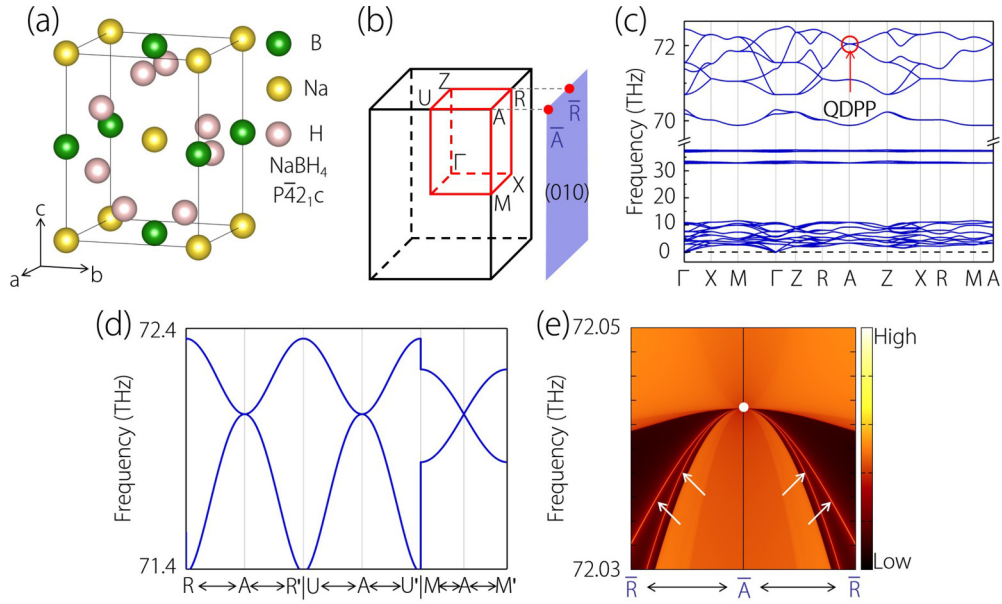
FIG. 4. (a) Crystal structure of $P\bar{4}2_1c$-type $NaBH_4$, (b) 3D BZ and 2D (010) surface BZ, (c) phonon dispersion of $NaBH_4$ along the Γ-X-M-Γ-Z-R-A-Z-X-R-M-A paths, (d) phonon dispersion along the R-A-R', U-A-U', M-A-M' paths, and (e) phonon LDOS projected on the (010) surface. The white arrows indicate the phonon surface states.

band splitting in the k_x-k_y plane (see examples of the phonon dispersions along the R-A-R' and U-A-U' paths in Fig. 4(d)). Figure 4(e) shows the phonon LDOS projected on the (010) surface. In Fig. 4(e), there are visible phononic surface states arising from the $\bar{A}$ point projections.

In addition to $P\bar{4}2_1c$-type $NaBH_4$, the other 437 material samples with SG numbers 106, 114, 124, 126, 128, 130, 133, 135, 137, 176, 184, 185, 186, 188, 190, 192, 193, 194, and 222, where QDPPs can also be found at HSPs, are included in Table S3 to support the inspired findings of the QDPPs.

VI. CCDPPS AT HSPS

As shown in Fig. 1(d), CCDPPs are zero-dimensional four-fold phonon band degeneracies with a topological charge of 0. CCDPPs [11] can be regarded as a combination of two C-4 Weyl points [94] with opposite topological charges. CCDPPs have a cubic crossing between two doubly degenerate bands along certain HSLs and a quadratic energy splitting in the plane normal to the HSLs. CCDPPs only appear at HSPs in the BZ. Following a screening of the encyclopedia of emergent particles [11], we discovered that the candidate SGs with numbers 218, 220, 222, 223, and 230 are the platforms for

obtaining CCDPPs at HSPs. Table V contains further information of the CCDPPs at HSPs in the SGs with the numbers 218, 220, 222, 223, and 230. In this section, as an example, we present the symmetry analysis for the CCDPP at HSPs in the SG with the number 230 as an example. For the materials with the $Ia\bar{3}d$ (SG No. 230), the CCDPP only appears at the H HSP in the 3D BZ. As shown in Table V, there are 4D irreps, R_8 and R_9, at this point, resulting in a fourfold Dirac point.

Different from previous examples, the reality of R_8 induced space group irreducible representation belongs to case (c) in Ref. [90]. That is, two different irreducible representation "stick together" by time-reversal symmetry. Then the matrix representation for unitary operations R and $\mathcal{T}$ can be written as

$$\mathcal{D}(R) = \begin{pmatrix} \Delta(R) & 0 \\ 0 & \Delta^*(\mathcal{T}^{-1}R\mathcal{T}) \end{pmatrix},$$

$$\mathcal{D}(\mathcal{T}) = \begin{pmatrix} 0 & \Delta(E) \\ \Delta(E^{-1}) & 0 \end{pmatrix}. \tag{11}$$

Therefore, we have

$$\mathcal{D}(C_{32}) = \tfrac{1}{2}(\Gamma_{00} - i\sqrt{3}\Gamma_{33}), \quad \mathcal{D}(C_{2x}) = \mathcal{D}(C_{2y}) = -\Gamma_{00},$$

$$\mathcal{D}(\sigma_{da}) = i\Gamma_{02}, \quad \mathcal{D}(P) = \Gamma_{03}, \quad \mathcal{D}(\mathcal{T}) = \Gamma_{10}\mathcal{K}. \tag{12}$$

TABLE V. A list of the CCDPPs at HSPs in the 230 SGs. The first and second columns contain the SG number and SG symbol, respectively. The third column shows the name of $\boldsymbol{k}$. The fourth and the fifth columns contain the IRRs of the LG and the GEs of the LG of $\boldsymbol{k}$, respectively. For more details, one can refer to Refs. [11,90].

218	$P\bar{4}3n$	R	$\{R_6, R_6\}$	$\{S_{4x}^+|\tfrac{1}{2}\tfrac{1}{2}\tfrac{1}{2}\}, \{\sigma_{da}|\tfrac{1}{2}\tfrac{1}{2}\tfrac{1}{2}\}, \{C_{33}^-|000\}, \mathcal{T}$
220	$I\bar{4}3d$	H	$\{R_6, R_6\}$	$\{S_{4x}^+|\tfrac{1}{2}00\}, \{\sigma_{da}|\tfrac{1}{2}00\}, \{C_{33}^-|0\tfrac{1}{2}\tfrac{1}{2}\}, \mathcal{T}$
222	$Pn\bar{3}n$	R	$\{R_8, R_9\}$	$\{C_{32}^-|000\}, \{C_{2x}|000\}, \{C_{2y}|000\}, \{C_{2f}|000\}, \{I|\tfrac{1}{2}\tfrac{1}{2}\tfrac{1}{2}\}, \mathcal{T}$
223	$Pm\bar{3}n$	R	$\{R_8, R_9\}$	$\{C_{32}^-|000\}, \{C_{2x}|000\}, \{C_{2y}|000\}, \{C_{2f}|\tfrac{1}{2}\tfrac{1}{2}\tfrac{1}{2}\}, \{I|000\}, \mathcal{T}$
230	$Ia\bar{3}d$	H	$\{R_8, R_9\}$	$\{C_{32}^-|\tfrac{1}{2}\tfrac{1}{2}0\}, \{C_{2x}|\tfrac{1}{2}\tfrac{1}{2}0\}, \{C_{2y}|0\tfrac{1}{2}\tfrac{1}{2}\}, \{\sigma_{da}|\tfrac{1}{2}00\}, \{I|000\}, \mathcal{T}$
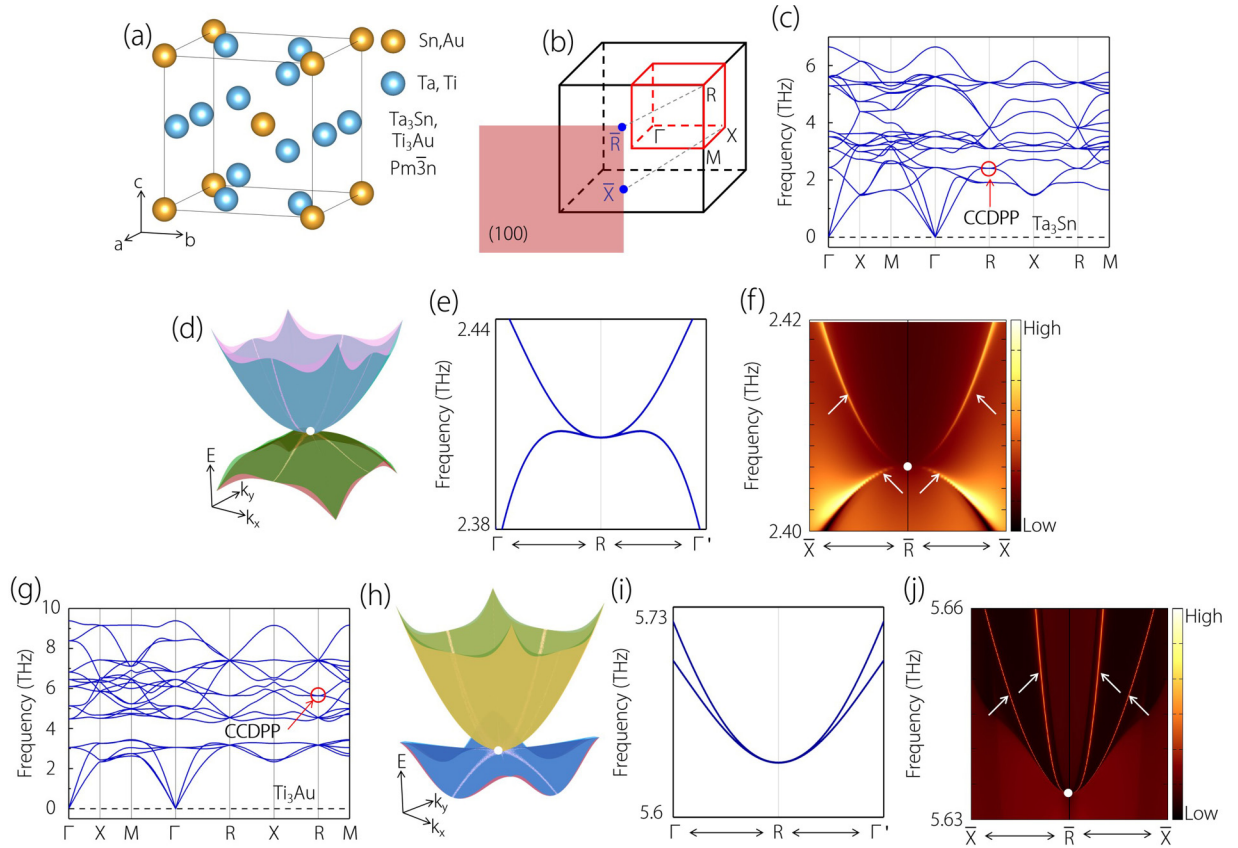
FIG. 5. (a) Crystal structure of $Pm\bar{3}n$-type Ti_3Au and Ta_3Sn, (b) 3D BZ and 2D (100) surface BZ, (c) phonon dispersion of Ta_3Sn along the Γ-X-M-Γ-R-X-R-M paths, (d) 3D phonon band dispersion of Ta_3Sn in the k_x-k_y plane, (e) phonon dispersion of Ta_3Sn along the Γ-R-Γ' paths ($k_{(111)}$ direction), and (f) phonon LDOS projected on the (100) surface for Ta_3Sn. The white arrows indicate the phonon surface states. (g) Phonon dispersion of Ti_3Au along the Γ-X-M-Γ-R-X-R-M paths, (h) 3D phonon band dispersion of Ti_3Au in the k_x-k_y plane, (i) phonon dispersion of Ti_3Au along the Γ-R-Γ' paths ($k_{(111)}$ direction), and (j) phonon LDOS projected on the (100) surface for Ti_3Au. The white arrows indicate phonon surface states.

Its corresponding effective Hamiltonian is given by

$$\mathcal{H}_{230}(\boldsymbol{k}) = w(\boldsymbol{k})\Gamma_{00} + \sqrt{3}(c_1\Gamma_{13} + c_2\Gamma_{23})(k_x^2 - k_y^2)$$
$$+ (c_2\Gamma_{10} - c_1\Gamma_{20})(k_x^2 + k_y^2 - 2k_z^3)$$
$$+ (c_3\Gamma_{12} + c_4\Gamma_{22})k_xk_yk_z, \qquad (13)$$

where $w(\boldsymbol{k}) = A + B(k_x^2 + k_y^2 + k_z^2)$. Remarkably, it has a cubic dispersion along the (111) direction. However, it has a quadratic dispersion within the plane normal to this direction. It is referred to as a CCDPP [95]. Furthermore, it has a cubic dispersion, but it has a topological charge of 0.

Furthermore, as shown in Table V, the CCDPP only appears at the R HSP in the $Pm\bar{3}n$ (SG No. 223). Two realistic materials have been created to study their CCDPPs in detail: Ti_3Au [96] and Ta_3Sn [97] with the $Pm\bar{3}n$ type structure. Ta_3Sn can be experimentally synthesized via an arc furnace reaction. Ti_3Au can be melted in an electric arc furnace using a nonconsumable tungsten electrode. Figure 5(a) depicts their crystal structures. Their phonon dispersions are calculated using the selected symmetry path Γ-X-M-Γ-R-X-R-M [see Fig. 5(b)], and the results are shown in Figs. 5(c) and 5(g). A CCDP can be observed at the R HSP (marked by a red circle) in Figs. 5(c) and 5(g). The order band splitting of the CCDP at the R HSP is cubic along the $k_{(111)}$ direction [see

Figs. 5(e) and 5(i)] and quadratic in the plane normal to the $k_{(111)}$ direction [see examples of 3D phonon bands in the k_x-k_y plane exhibited in Figs. 5(d) and 5(h)]. It is worth noting that materials with fourfold DPPs and cubic band crossings have not been previously reported. As shown by the phonon LDOS projected on the (100) surface exhibited in Figs. 5(f) and 5(j), the phonons surface states (white arrows) arise from the $\bar{R}$ point for both materials.

Table S4 lists 110 material candidates that host CCDPPs at HSPs to support the inspired findings of the CCDPPs at HSPs. The CCDPPs in these materials are symmetry dominated, and the corresponding irreps and generators of the CCDPPs at HSPs in each SG can be found in Table V.

VII. ADDITIONAL NOTES

Before closing, we would like to present some additional notes as follows. (1) Although more than 1000 candidates are proposed to be the hosts with DPPs at HSPs, not all the materials are ideal. Hence, continued follow-up investigation of searching for ideal materials with obvious DPPs and clearly visible surface states remain essential to the researchers. Note that the NiSbS belongs to the ideal materials with visible surface states. We exhibit the isofrequency surface contours at 7.45 THz [see Fig. 3(e)]. Corresponding to the obtained

topological charge of the C-2 DPP, as expected, double arc-shaped surface states are emanating from the projection of the C-2 DPP (i.e., $\bar{R}$ point).

(2) When the polariton of longitudinal optical-transverse optical (LO-TO) splitting is added, the longitudinal branch in the phononic spectra may become discontinuous around the Γ point. There is because the dipoles from the charge displacement of the long-wavelength LO mode create an electric field [98]. Away from this point, the polariton of LO-TO splitting does not break any phonon branch. Hence, the reported DPPs at HSPs should still exist when considering the polariton of LO-TO splitting due to the DPPs not appearing at the Γ point (see Tables II–V). As examples, the enlarged phonon dispersions for Li_3AsS_3, NiSbS, $NaBH_4$, Ti_3Au, and Ta_3Sn with LO-TO splitting are shown in Fig. S2 (see the SM [86]). One finds that the DDPs at HSPs still exist, supporting their robustness to the polariton of LO-TO splitting.

(3) Besides the DPPs with the essential degeneracies at HSPs, the DPPs with the accidental degeneracies on HSLs have also been reported by Yu *et al.* [11] and Chen *et al.* [63]. In this work we also screened the encyclopedia of emergent particles [11] and exhibited the candidate SGs that can host DPPs on HSLs (see Table S5 in the SM [86]). It is still challenging to search for ideal material candidates with DPPs on HSLs. In this work, three realistic materials, BaS_3, NiAsS, and MgF_2, with QDPP on the *A-M*, C-2 DPP on the *R-M*, and C-0 DPP on the *X-M* HSLs, respectively, are selected as examples. The results are shown in Fig. S3 [86].

(4) Using NiSbS as an example, we checked the influence of the on-site Coulomb interaction (U) on the Dirac phonons by applying the effective $U = 4$ eV for Ni-p and Ni-d orbitals. The results are shown in Figs. S4(b) and S4(c) [86], respectively. The calculated results show that the C-2 DPP at *R* HSP is robust to the U effect.

(5) Using Ti_3Au as an example, we examined the influence of the spin-orbit coupling (SOC) on the Dirac phonons of materials containing heavy elements. The result is shown in Fig. S4(e) [86]. Obviously the SOC has no effect on the Dirac phonons at HSPs.

(6) We exhibited the phonon dispersions for all the material candidates (listed in Tables S1, S2, S3, S4) in Figs. S5– S1271 [86]. One can find the phonon dispersion and the type of DPPs for each material based on the SG number in the SM [86].

VIII. CONCLUSIONS

To summarize, we screened the encyclopedia of emergent particles [11] and identified the candidate SGs with DPPs at HSPs. In detail, SGs with the numbers 29, 33, 52, 54, 56, 60, 73, 103, 104, 110, 130, 138, 142, 158, 159, 161, 163, 165, 167, 184, 185, 192, 193, 206, 219, 220, 226, 228, and 230 are the platforms for obtaining C-0 DPPs at HSPs. SGs with numbers 19, 92, 96, 198, 212, and 213 are the platforms for obtaining C-2 DPPs at HSPs. SGs with numbers 106, 114, 124, 126, 128, 130, 133, 135, 137, 176, 184, 185, 186, 188, 190, 192, 193, 194, and 222 host QDPPs at HSPs. SGs with numbers 218, 220, 222, 223, and 230 can contain CCDPPs at HSPs. The candidate SGs can be used to search for or design topological phononic materials with different types of Dirac points because these DPPs at HSPs are symmetry enforced. Herein we propose five realistic materials with different types of Dirac points in their phonon dispersions using the first-principles calculations: $Pna2_1$-type Li_3AsS_3, which has a C-0 DPP at the *T* HSP, $P2_13$-type NiSbS, which has a C-2 DPP at the *R* HSP, $P\bar{4}2_1c$-type $NaBH_4$, which has a QDDP at the *A* HSP, and $Pm\bar{3}n$-type Ti_3Au and Ta_3Sn, which have a QCDDP at the *R* HSP. The phononic surface states of these five materials are exhibited. Furthermore, we exhibited 644 candidates with C-0 DPPs, 183 candidates with C-2 DPPs, 438 candidates with QDPPs, and 110 candidates with CCDPPs at HSPs. Therefore, our findings can serve as a general guideline for investigating DPPs in solid-state materials.

[1] B. Yan and S.-C. Zhang, Rep. Prog. Phys. **75**, 096501 (2012).

[2] M. G. Vergniory, L. Elcoro, C. Felser, N. Regnault, B. A. Bernevig, and Z. Wang, Nature (London) **566**, 480 (2019).

[3] B. Yan and C. Felser, Annu. Rev. Condens. Matter Phys. **8**, 337 (2017).

[4] S.-S. Wang, Y. Liu, Z.-M. Yu, X.-L. Sheng, and S. Y. A. Yang, Nat. Commun. **8**, 1844 (2017).

[5] S. A. Yang, SPIN **06**, 1640003 (2016).

[6] A. A. Burkov, Nat. Mater. **15**, 1145 (2016).

[7] J. Hu, S.-Y. Xu, N. Ni, and Z. Mao, Annu. Rev. Mater. Res. **49**, 207 (2019).

[8] H. Weng, X. Dai, and Z. Fang, J. Phys.: Condens. Matter **28**, 303001 (2016).

[9] H. Gao, J. W. F. Venderbos, Y. Kim, and A. M. Rappe, Annu. Rev. Mater. Res. **49**, 153 (2019).

[10] B. Q. Lv, T. Qian, and H. Ding, Rev. Mod. Phys. **93**, 025002 (2021).

[11] Z.-M. Yu, Z. Y. Zhang, G.-B. Liu, W. K. Wu, X.-P. Li, R.-W. Zhang, S. Y. A. Yang, and Y. G. Yao, Sci. Bull. **67**, 375 (2022).

[12] Z.-M. Yu, Y. Yao, and S. A. Yang, Phys. Rev. Lett. **117**, 077202 (2016).

[13] X. Zhang, Z.-M. Yu, X.-L. Sheng, H. Y. Yang, and S. A. Yang, Phys. Rev. B **95**, 235116 (2017).

[14] B. Q. Lv, H. M. Weng, B. B. Fu, X. P. Wang, H. Miao, J. Ma, P. Richard, X. C. Huang, L. X. Zhao, G. F. Chen *et al.*, Phys. Rev. X **5**, 031013 (2015).

[15] Y. Sun, S.-C. Wu, and B. Yan, Phys. Rev. B **92**, 115428 (2015).

[16] Y. Sun, Y. Zhang, C. Felser, and B. Yan, Phys. Rev. Lett. **117**, 146403 (2016).

[17] S.-M. Huang, S.-Y. Xu, I. Belopolski, C.-C. Lee, G. Chang, B. Wang, N. Alidoust, G. Bian, M. Neupane, A. Bansil *et al.*, Nat. Commun. **6**, 7373 (2015).

[18] N. P. Armitage, E. J. Mele, and A. Vishwanath, Rev. Mod. Phys. **90**, 015001 (2018).

[19] Q. D. Gibson, L. M. Schoop, L. Muechler, L. S. Xie, M. Hirschberger, N. P. Ong, R. Car, and R. J. Cava, Phys. Rev. B **91**, 205128 (2015).

[20] T.-R. Chang, S.-Y. Xu, D. S. Sanchez, W.-F. Tsai, S.-M. Huang, G. Chang, C.-H. Hsu, G. Bian, I. Belopolski, Z.-M. Yu, S. A. Yang, T. Neupert, H.-T. Jeng, H. Lin, and M. Z. Hasan, Phys. Rev. Lett. **119**, 026404 (2017).

[21] Z. Zhu, Z.-M. Yu, W. Wu, L. Zhang, W. Zhang, F. Zhang, and S. A. Yang, Phys. Rev. B **100**, 161401(R) (2019).

[22] C. Chen, S.-S. Wang, L. Liu, Z.-M. Yu, X.-L. Sheng, Z. Chen, and S. A. Yang, Phys. Rev. Mater. **1**, 044201 (2017).

[23] S. Li, Y. Liu, S.-S. Wang, Z.-M. Yu, S. Guan, X.-L. Sheng, Y. Yao, and S. A. Yang, Phys. Rev. B **97**, 045131 (2018).

[24] T.-T. Zhang, Z.-M. Yu, W. Guo, D. Shi, G. Zhang, and Y. Yao, J. Phys. Chem. Lett. **8**, 5792 (2017).

[25] S. Li, Y. Liu, Z.-M. Yu, Y. Jiao, S. Guan, X.-L. Sheng, Y. Yao, and S. A. Yang, Phys. Rev. B **100**, 205102 (2019).

[26] W. Wu, Z.-M. Yu, X. Zhou, Y. X. Zhao, and S. A. Yang, Phys. Rev. B **101**, 205134 (2020).

[27] C. K. Barman, C. Mondal, B. Pathak, and A. Alam, Phys. Rev. B **99**, 045144 (2019).

[28] Z. Zhu, G. W. Winkler, Q. S. Wu, J. Li, and A. A. Soluyanov, Phys. Rev. X **6**, 031003 (2016).

[29] N. Kumar, Y. Sun, M. Nicklas, S. J. Watzman, O. Young, I. Leermakers, J. Hornung, J. Klotz, J. Gooth, K. Manna, V. Süß, S. N. Guin, T. Förster, M. Schmidt, L. Muechler, B. Yan, P. Werner, W. Schnelle, U. Zeitler, J. Wosnitza, S. S. P. Parkin, C. Felser *et al.*, Nat. Commun. **10**, 2475 (2019).

[30] Z. P. Sun, C. Q. Hua, X. L. Liu, Z. T. Liu, M. Ye, S. Qiao, Z. H. Liu, J. S. Liu, Y. F. Guo, Y. H. Lu, and D. W. Shen, Phys. Rev. B **101**, 155114 (2020).

[31] N. B. M. Schröter, D. Pei, M. G. Vergniory, Y. Sun, K. Manne, F. d. Juan, J. A. Krieger, V. Süss, M. Schmidt, P. Dudin, B. Bradlyn, T. K. Kim, T. Schmitt, C. Cacho, C. Felser, V. N. Strocov, and Y. Chen, Nat. Phys. **15**, 759 (2019).

[32] N. Kumar, M. Yao, J. Nayak, M. G. Vergniory, J. Bannies, Z. Wang, N. B. M. Schrötter, V. N. Strocov, L. Mötchler, W. Shi, E. D. L. Rienks, J. L. Maôes, C. Shekhar, S. S. P. Parkin, J. Fink, G. H. Fecher, Y. Sun, B. A. Bernevig, and C. Felser, Adv. Mater. **32**, 1906046 (2020).

[33] B. Bradlyn, J. Cano, Z. Wang, M. G. Vergniory, C. Felser, R. J. Cava, and B. A. Bernevig, Science **353**, aaf5037 (2016).

[34] S. Nie, B. A. Bernevig, and Z. Wang, Phys. Rev. Res. **3**, L012028 (2021).

[35] B. J. Wieder, Y. Kim, A. M. Rappe, and C. L. Kane, Phys. Rev. Lett. **116**, 186402 (2016).

[36] H. Weng, C. Fang, Z. Fang, and X. Dai, Phys. Rev. B **93**, 241202(R) (2016).

[37] H. Weng, C. Fang, Z. Fang, and X. Dai, Phys. Rev. B **94**, 165201 (2016).

[38] C. Fang, Y. Chen, H.-Y. Kee, and L. Fu, Phys. Rev. B **92**, 081201(R) (2015).

[39] D.-S. Ma, J. Zhou, B. Fu, Z.-M. Yu, C.-C. Liu, and Y. Yao, Phys. Rev. B **98**, 201104(R) (2018).

[40] X.-P. Li, B. Fu, D.-S. Ma, C. Cui, Z.-M. Yu, and Y. Yao, Phys. Rev. B **103**, L161109 (2021).

[41] F. Zhou, C. X. Cui, J. H. Wang, M. Q. Kuang, T. Yang, Z.-M. Yu, X. T. Wang, G. Zhang, and Z. X. Cheng, Phys. Rev. B **103**, 245126 (2021).

[42] Z. Zhang, Z.-M. Yu, and S. A. Yang, Phys. Rev. B **103**, 115112 (2021).

[43] X.-L. Sheng, Z.-M. Yu, R. Yu, H. Weng, and S. A. Yang, J. Phys. Chem. Lett. **8**, 3506 (2017).

[44] X. M. Zhang, Z.-M. Yu, Z. M. Zhu, W. K. Wu, S.-S. Wang, X.-L. Sheng, and S. A. Yang, Phys. Rev. B **97**, 235150 (2018).

[45] C. Chen, Z.-M. Yu, S. Li, Z. Chen, X.-L. Sheng, and S. A. Yang, Phys. Rev. B **99**, 075131 (2019).

[46] Z.-M. Yu, W. K. Wu, X.-L. Sheng, Y. X. Zhao, and S. Y. A. Yang, Phys. Rev. B **99**, 121106(R) (2019).

[47] W. Wu, Y. Liu, S. Li, C. Zhong, Z.-M. Yu, X.-L. Sheng, Y. X. Zhao, and S. A. Yang, Phys. Rev. B **97**, 115125 (2018).

[48] S. Z. Chen, S. Li, Y. Chen, and W. Duan, Nano Lett. **20**, 5400 (2020).

[49] Q.-F. Liang, J. Zhou, R. Yu, Z. Wang, and H. Weng, Phys. Rev. B **93**, 085427 (2016).

[50] C. Zhong, Y. Chen, Y. Xie, S. A. Yang, M. L. Cohen, and S. Zhang, Nanoscale **8**, 7232 (2016).

[51] B. W. Xia, R. Wang, Z. J. Chen, Y. J. Zhao, and H. Xu, Phys. Rev. Lett. **123**, 065501 (2019).

[52] J. Liu, W. Hou, E. Wang, S. Zhang, J.-T. Sun, and S. Meng, Phys. Rev. B **100**, 081204(R) (2019).

[53] J. X. Li, Q. Xie, S. Ullah, R. H. Li, H. Ma, D. Z. Li, Y. Y. Li, and X.-Q. Chen, Phys. Rev. B **97**, 054305 (2018).

[54] P. F. Liu, J. Li, X. H. Tu, H. Li, J. Zhang, P. Zhang, Q. Gao, and B. T. Wang, Phys. Rev. B **103**, 094306 (2021).

[55] T. T. Zhang, Z. D. Song, A. Alexandradinata, H. M. Weng, C. Fang, L. Lu, and Z. Fang, Phys. Rev. Lett. **120**, 016401 (2018).

[56] Q.-B. Liu, Z. Wang, and H.-H. Fu, Phys. Rev. B **103**, L161303 (2021).

[57] Y. J. Jin, Z. J. Chen, X. L. Xiao, and H. Xu, Phys. Rev. B **103**, 104101 (2021).

[58] Q.-B. Liu, Y. Qian, H.-H. Fu, and Z. Wang, Npj Comput. Mater. **6**, 95 (2020).

[59] R. Wang, B. W. Xia, Z. J. Chen, B. B. Zheng, Y. J. Zhao, and H. Xu, Phys. Rev. Lett. **124**, 105303 (2020).

[60] Z. Huang, Z. Chen, B. Zheng, and H. Xu, Npj Comput. Mater. **6**, 87 (2020).

[61] S. Singh, Q. S. Wu, C. M. Yue, A. H. Romero, and A. A. Soluyanov, Phys. Rev. Mater. **2**, 114204 (2018).

[62] C. W. Xie, Y. Liu, Z. Y. Zhang, F. Zhou, T. Yang, M. Q. Kuang, X. T. Wang, and G. Zhang, Phys. Rev. B **104**, 045148 (2021).

[63] Z. J. Chen, R. Wang, B. W. Xia, B. B. Zheng, Y. J. Jin, Y.-J. Zhao, and H. Xu, Phys. Rev. Lett. **126**, 185301 (2021).

[64] G. Liu, Y. Jin, Z. Chen, and H. Xu, Phys. Rev. B **104**, 024304 (2021).

[65] F. Zhou, Z. Y. Zhang, H. Chen, M. Q. Kuang, T. Yang, and X. T. Wang, Phys. Rev. B **104**, 174108 (2021).

[66] Q.-B. Liu, H.-H. Fu, and R. Wu, Phys. Rev. B **104**, 045409 (2021).

[67] J. Li, L. Wang, J. Liu, R. Li, Z. Zhang, and X.-Q. Chen, Phys. Rev. B **101**, 081403(R) (2020).

[68] B. Zheng, F. Zhan, X. Wu, R. Wang, and J. Fan, Phys. Rev. B **104**, L060301 (2021).

[69] T. T. Zhang, H. Miao, Q. Wang, J. Q. Lin, Y. Cao, G. Fabbris, A. H. Said, X. Liu, H. C. Lei, Z. Fang, H. M. Weng, and M. P. M. Dean, Phys. Rev. Lett. **123**, 245302 (2019).

[70] Y. J. Jin, Z. J. Chen, B. W. Xia, Y. J. Zhao, R. Wang, and H. Xu, Phys. Rev. B **98**, 220103(R) (2018).

[71] B. Peng, S. Murakami, B. Monserrat, and T. T. Zhang, Npj Comput. Mater. **7**, 195 (2021).

[72] J.-Y. You, X.-L. Sheng, and G. Su, Phys. Rev. B **103**, 165143 (2021).

[73] Q.-B. Liu, Z.-Q. Wang, and H.-H. Fu, Phys. Rev. B **104**, L041405 (2021).

[74] C. W. Xie, H. K. Yuan, Y. Liu, X. T. Wang, and G. Zhang, Phys. Rev. B **104**, 134303 (2021).

[75] H. Miao, T. T. Zhang, L. Wang, D. Meyers, A. H. Said, Y. L. Wang, Y. G. Shi, H. M. Weng, Z. Fang, and M. P. M. Dean, Phys. Rev. Lett. **121**, 035302 (2018).

[76] J. Li, J. Liu, S. A. Baronett, M. Liu, L. Wang, and R. Li, Y. Chen, D. Li, Q. Zhu, and X.-Q. Chen, Nat. Commun. **12**, 1204 (2021).

[77] X. Q. Chen, J. X. Liu, and J. X. Li, The Innovation **2**, 100134 (2021).

[78] http://phonondb.mtl.kyoto-u.ac.jp/.

[79] https://icsd.products.fiz-karlsruhe.de/.

[80] R. G. Parr, Annu. Rev. Phys. Chem. **34**, 631 (1983).

[81] J. Hafner, J. Comput. Chem. **29**, 2044 (2008).

[82] J. P. Perdew, K. Burke, and M. Ernzerhof, Phys. Rev. Lett. **80**, 891 (1998).

[83] P. E. Blöchl, Phys. Rev. B **50**, 17953 (1994).

[84] A. Togo and I. Tanaka, Scr. Mater. **108**, 1 (2015).

[85] Q. Wu, S. Zhang, H.-F. Song, M. Troyer, and A. A. Soluyanov, Comput. Phys. Commun. **224**, 405 (2018).

[86] See Supplemental Material at http://link.aps.org/supplemental/ 10.1103/PhysRevB.106.134307 for enlarged phonon dispersions for Li_3AsS_3, NiSbS, $NaBH_4$, Ti_3Au, and Ta_3Sn with LO-TO splitting, the quality of the Wannier functions for the five materials, phonon dispersions for NiSbS with $U = 4$ eV for Ni-d and Ni-p orbitals, phonon dispersion for Ti_3Au with SOC, three material candidates with the DPPs on HSLs, Refs [78,79,87–89] therein, and the phonon disperisons for 644 candidates with C-0 DPPs, 183 candidates with C-2 DPPs, 438 candidates with QDPPs, and 110 candidates with CCDPPs at HSPs.

[87] N. K. Goh, Naturwissenschaften **61**, 272 (1974).

[88] Y. Takéuchi, Mineralog. J. **2**, 90 (1957).

[89] W. H. Baur, Acta Crystallogr. Sect. B **32**, 2200 (1976).

[90] C. J. Bradley and A. P. Cracknell, *The Mathematical Theory of Symmetry in Solids: Representation Theory for Point Groups and Space Groups* (Oxford University Press, New York, 2009).

[91] S. Huber, C. Preitschaft, R. Weihrich, and A. Pfitzner, Z. Anorg. Allg. Chem. **638**, 2542 (2012).

[92] A. J. Foecker and W. Jeitschko, J. Solid State Chem. **162**, 69 (2001).

[93] E. Kim, R. Kumar, P. F. Weck, A. L. Cornelius, M. Nicol, S. C. Vogel, J. Zhang, M. Hartl, A. C. Stowe, L. Daemen, and Y. Zhao, J. Phys. Chem. B **111**, 13873 (2007).

[94] C. X. Cui, X.-P. Li, D.-S. Ma, Z.-M. Yu, and Y. G. Yao, Phys. Rev. B **104**, 075115 (2021).

[95] Z. Zhang, Z.-M. Yu, G.-B. Liu, and Y. Yao, arXiv:2201.11350.

[96] E. C. van Reuth and R. M. Waterstrat, Acta Crystallogr. Sect. B **24**, 186 (1968).

[97] S. Geller and B. T. Matthias, J. Am. Chem. Soc. **77**, 1502 (1955).

[98] W. Zhong, R. D. King-Smith, and D. Vanderbilt, Phys. Rev. Lett. **72**, 3618 (1994).